5
FIELD TRIALS

5.1 INTRODUCTION

The previous chapter examined the relationship between the microstructure of a single-bead deposit and its abrasive wear performance, as measured under laboratory test conditions. After the laboratory testing was completed a plan was developed for a series of field trials. The aim of the trials was to establish whether there is a correlation between the results of laboratory wear testing and the wear performance observed in the field.

Two trials were initiated. The first involved depositing a range of hardfacing overlays on to a pair of wear plates that were to be put into service at a quartz quarry. The second involved depositing a similar range of overlays on to sets of plates that were to be used in a jaw crusher. In each case, the intention was to test several different microstructures under nominally identical service conditions.

The two dominant influences on the wear performance of an overlay are the geometry of the deposit and its microstructure. In order to isolate the effects of microstructure it is necessary to achieve the same geometry in each deposit, yet still vary the microstructure for each overlay. Such a constraint would require each overlay to have the same height, width and length, but a different penetration so that in each case the dilution would be different. These experiments are believed to be the first of their kind. They presented

many challenges and required very careful selection of welding parameters. The purpose of this chapter is to describe the experiments and their significance.

5.2 THE HEEL PLATES EXPERIMENT

5.2.1 Description of Experiment

Five single-layer overlays were deposited on each of a pair of heel plates for the excavation bucket of a Caterpillar 988F wheel loader. The plate dimensions were 680mm by 254mm and the thickness was 25.4mm. Four different sets of welding parameters were used. The sets of parameters were selected in such a way that they achieved four different microstructures, yet the pad dimensions were nominally identical at 200mm by 60mm and 5 ± 0.5mm high. Table 5.1 summarises the conditions that were used and the microstructures that were achieved.

Figure 5.1 shows a heel plate before it was put into service. The same welding consumable was used for all of the overlays. The consumable will be referred to as consumable B (described in section 3.2). Direct-current-electrode-positive polarity was used in all cases. Preheat temperatures were determined in accordance with the properties of the base steel from published data by WTIA : Technical Note 1 (1996). The preheat temperature required for condition 1 is higher due to the lower heat input.

In order to maintain flatness of the heel plates and to facilitate their subsequent bolting on to the bucket they were restrained by clamping during welding. The clamps were released after cooling. The ends of each pad were then ground so that, for each pad, there was a ramped transition from the substrate to full overlay height. The plates were bolted on to the lower surface of a wheel loader excavation bucket and put into service at

Boral's quartz quarry, Stonyfell, South Australia (see Figure 5.2). The service conditions would best be described as highly abrasive with moderate impact. The plates remained in service for 174 operating hours before they were removed for examination.

Overlay No.	Voltage	Current (A)	Speed (mm/min)	Work Dist. (mm)	Step (mm)	Height (mm)	Preheat (^{o}C)	Microstructure
1	**25**	**230**	**240**	**40**	**8**	**5.0**	**115**	Hypereutectic (hvf)
2	**33**	**410**	**380**	**40**	**10**	**5.0**	**60**	Eutectic
3	**36**	**490**	**270**	**30**	**19**	**4.5**	**60**	Hypoeutectic
4	**33**	**410**	**380**	**40**	**10**	**5.0**	**60**	Eutectic
5	**30**	**370**	**310**	**40**	**10**	**5.5**	**60**	Hypereutectic (lvf)

Table 5.1: - A summary of the heel plate welding conditions. These conditions were selected to achieve specific microstructures and are not necessarily suggested operating conditions. The 'hvf' and 'lvf' refer to high volume fraction and low volume fraction of primary carbides respectively. The average heights were obtained from an additional set of overlays that were deposited on a set of test plates (described in the next section), to avoid cutting the heel plates. Preheats were not used for the test plate overlays but, otherwise, the welding parameters were identical to those listed above.

Figure 5.1: - A heel plate before service.

Figure 5.2: - The arrows show the location of the heel plates on the excavation bucket of the Caterpillar 988F wheel loader.

Conditions 2 and 4 in Table 5.1 were identical and served as reference overlays. If the wear pattern on the plates were to be biased to one side this bias should be discernible from a comparison of the reference deposits.

5.2.2 Methodology for Selecting Welding Parameters

The intention with overlay number 1 was to achieve a hypereutectic microstructure with a high volume fraction of primary carbide needles. It was necessary to have a low dilution in order to obtain such a microstructure. Consequently, a low voltage was chosen in accordance with the findings of previous studies (summarised in Table 2.1 – page 10) and the model for single-bead dilution (see sections 2.2.3 and 3.6). A low welding current was also selected in view of the fact that, for a multi-pass overlay of a specified height, it is the average penetration, rather than the single-bead dilution, that

needs to be minimised. (The average dilution of a multi-pass deposit can be determined metallographically from the average height and average penetration of the deposit, as shown in Figure 5.3.) This realisation was one of great importance. It suggested that the optimum conditions for single beads may not necessarily correspond to the optimum conditions for multi-pass overlays. For a single-bead deposit it is the ratio of material deposited to material melted that is critical, and there is usually no restriction on the height of the bead. The height of a multi-pass overlay, however, is usually specified before the overlay is deposited. The average height is directly proportional to the consumable costs and is thus an important constraint. It is a constraint that also makes the philosophy for depositing multi-pass overlays and single beads fundamentally different. This issue is addressed in chapters 6 and 7.

In order of increasing dilution the overlay numbers were 1, 5, 2 (and 4), 3. In each case an increase in dilution was achieved by increasing the welding current and voltage as required. The welding current has a greater influence on average overlay dilution. The average penetration (see section 3.4) and deposition rate (see equation 2.4 – page 12) both increase with increasing current. An increase in penetration will result in a higher average dilution if the overlay height remains unchanged. The deposition rate effects, however, are not as obvious. As the deposition rate increases, the step-over needs to be increased in order to maintain the required overlay height. This results in a reduction in bead overlap and a corresponding shift in arc impingement away from the previous bead toward unmelted substrate, thus increasing dilution.

All of the selected welding conditions were first tested on 25.4mm thick steel substrates. After the test overlays were deposited they were sectioned, polished and etched with

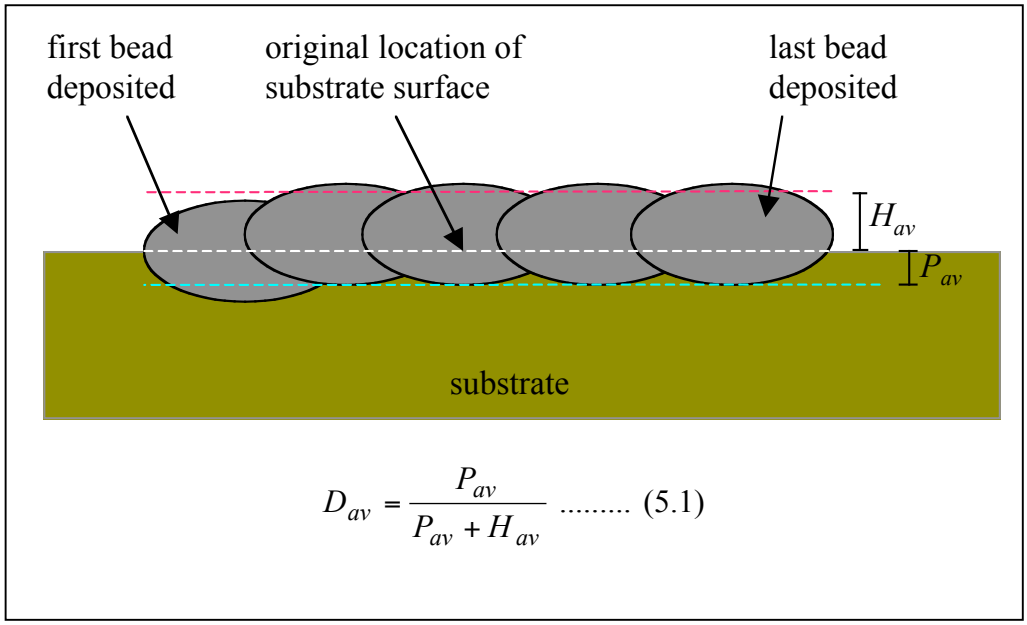

Figure 5.3: - The metallographic measurement of the average dilution of a multi-pass overlay. H_{av} and P_{av} are the average height and penetration for the deposit respectively.

Vilella's reagent so that average dilutions could be measured. The microstructure of each deposit was then examined using an optical microscope. Small adjustments to the welding parameters were required to ensure that, in each case, the desired microstructure was achieved. The tests were then repeated, and the microstructures were once again examined before deposition commenced on the heel plates. The microstructures of the test plates are shown in Figures 5.4.

The complete heel plate deposits were then examined using an in-situ metallographic technique. A small area, approximately 10mm by 10mm, on the surface of each deposit was ground smooth with a grinder and polished with 5□m diamond paste. The prepared surfaces were then placed on an inverted-stage optical microscope. All microstructures were similar to those shown for the test plates in Figures 5.4.

5.2.3 Achieving the Specified Overlay Height

It was mentioned in the previous section that the average height of an overlay would usually be specified before the overlay is deposited. In practice, the average height of the overlay under steady-state conditions is specified.

Consider the case where an overlay of steady-state height, H_{ss}, is to be deposited on a flat plate of breadth, B, and length, L, with open-arc FCAW. The configuration is shown schematically in Figure 5.5. Let it be assumed that a steady-state condition is achieved before deposition commences on the plate, for example, by the incorporation of a run-on plate.

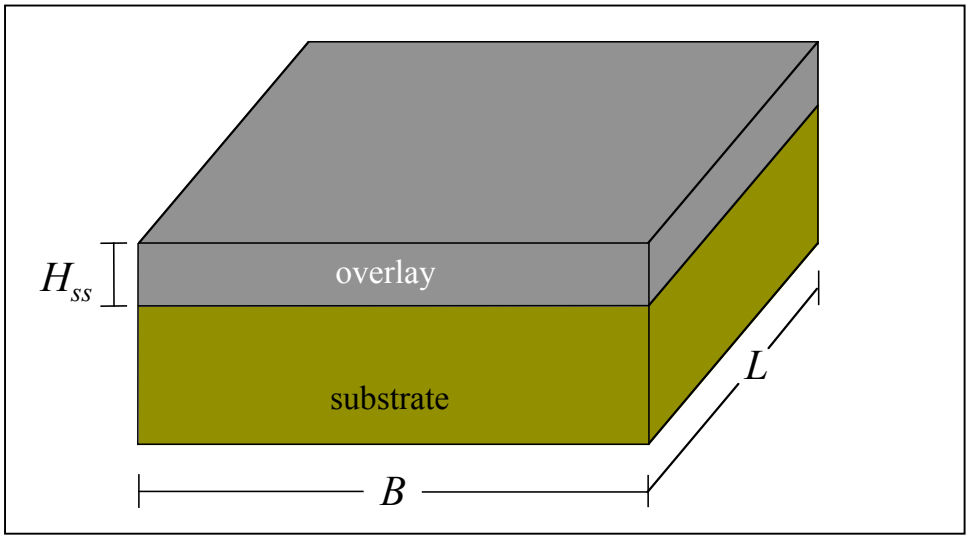

Figure 5.5: - The configuration of an overlay. The steady-state height, H_{ss}, does not include the depth of penetration.

There will be three major influences on the steady-state overlay height, namely:

- The deposition rate, W
- The travel speed, S
- The step-over, $\square$

The deposition rate, W, is given by:

$$W = \varsigma_d f m \quad \cdots\cdots\cdots (5.2)$$

where $\square_d$ is the deposition efficiency, m is the mass per unit length of the welding consumable and f is the wire feed rate. For the high-chromium high-carbon consumables studied in this work, the deposition efficiencies were high (see section 3.7), with typical values falling between 95 and 98%. It would therefore be reasonable to assume a deposition efficiency of 95% for similar consumables. The mass per unit length of wire, m, is readily obtained from the manufacturers' data sheets or by direct measurement and the wire feed speed is usually set by the operator and recorded on the welding procedure sheet. Thus, all of the information required to estimate the deposition rate is available.

The travel speed is another parameter set by the operator and recorded on the welding procedure sheet. Consequently the step-over, $\square$, is the only remaining parameter that needs to be determined in order to achieve the correct overlay height, and it can be obtained by applying the principle of conservation of mass.

The total mass added to the plate will be equal to the product of the added volume and the density of an all-weld-metal deposit, $\square$. It will also be equal to the product of the deposition rate, W, and the total welding time, t. Thus we have the following relationship:

$$W t = \tilde{n} L B H_{ss} \quad \cdots\cdots\cdots (5.3)$$

The total welding time can be expressed in terms of the number of passes required to cover the plate, N, the length of the plate, L, and the welding speed, S.

$$t = N\frac{L}{S} \quad \text{..... (5.4)}$$

Under steady-state conditions the number of passes required to cover the plate, N, is given by dividing the plate width, B, by the step-over, $\square$, *i.e.*:

$$N = \frac{B}{\square}$$

Substituting for N in equation 5.4, and then substituting equation 5.4 into 5.3 gives:

$$\ddot{a} = \frac{W}{\tilde{n}\, H_{ss}\, S} \quad \text{.....} \quad (5.5)$$

Equation 5.5 may be used in conjunction with equation 5.2 to determine the step-over that will give the desired steady-state overlay height for a given set of welding parameters. Alternatively, it will predict the steady-state height for a given step-over. This equation gives the correct average height but does not give any indication of the overlay uniformity. Equation 5.5 requires all parameters to be entered in SI units.

5.2.4 Results

Visual examination showed that, whereas all pads revealed some wear, the hypereutectic deposits showed an incidence of metal loss by spalling. Spalling was worst on the deposits that had a high volume fraction of primary carbides, but also occurred on the overlays with low volume fractions. In all cases spalling had initiated at the corner of the overlay deposit. There was no evidence of spalling on the eutectic or hypoeutectic samples.

In order to get an indication of abrasion resistance, volume loss measurements were performed on those areas of each pad that had not spalled. It was found that only small amounts of each pad had been removed by abrasion and that substantially more service time would have been required in order to obtain meaningful abrasive wear data.

Figure 5.6 shows the condition of a heel plate after 174 hours service. Conditions 1 to 5 (in Table 5.1) appear from left to right respectively. It can be seen that the bottom left hand corner of the left-most deposit has completely disappeared. Spalling has also commenced on the right-most deposit, with the top-left and bottom-left corners being removed.

Figure 5.6: - A heel plate after service.

5.3 THE JAW-CRUSHER EXPERIMENT

5.3.1 Description of Experiment

The heel plates experiment was followed by a jaw-crusher experiment. The welding parameters listed in Table 5.1 were once again employed, with the exception of condition 1, which was replace by a welding condition that had a higher overlap in order to reduce dilution. In this instance the overlays were deposited on a set of jaw-crusher plates approximately 220mm long, 75mm wide and 25mm thick. Two different batches of welding consumable were used and, as a result, the microstructures were not identical to those produced in the heel plates experiment. Nevertheless, four different microstructures were produced.

This trial was conducted with the assistance of a project team that had previous experience with jaw crusher tests. The clad plates were tested in the as-deposited surface condition as stationary and moving half jaws in a single-toggle crusher in accordance with the procedure described in ASTM Standard G81-83. Each plate was used to crush 1000kg of quartzite-bearing rock, designated "ANR Ballast", in the size range 25 – 50mm. It was necessary to increase the jaw opening in order to accommodate the size of the rock and to ensure correct operation of the crusher. The same jaw opening was, however, used in all tests and the results were compared to those for a quenched and tempered steel, which served as a reference material. The test strategy was based on the work of Sare and Constantine (1991). The wear mechanism in this type of test is believed to be gouging abrasion.

5.3.2 Results

Table 5.2 summarises the weight losses for each microstructure. The data suggest that the best wear performance, in this particular application, is offered by microstructures that are either near-eutectic or hypereutectic with a low volume fraction of primary carbides. Typical wear surfaces for both stationary and moving jaws are shown in Figures 5.7(a) and 5.7(b) respectively. It can be seen that the low-dilution deposits, *i.e.* those with high primary carbide volume fractions, developed the greatest number of check cracks. These samples were also the most susceptible to accelerated metal loss by spalling.

Microstructure	Weight Loss, g (Stationary Jaw)	Weight Loss, g (Moving Jaw)
Hypoeutectic	17	12
Eutectic to near-eutectic	15	11
Hypereutectic – lvf	16	9
Hypereutectic – hvf	23	13
Reference material	50	36

Table 5.2: - The average weight losses in grams for each type of microstructure in the jaw-crusher tests. "lvf" and "hvf" refer to low volume fraction and high volume fraction of primary carbides respectively.

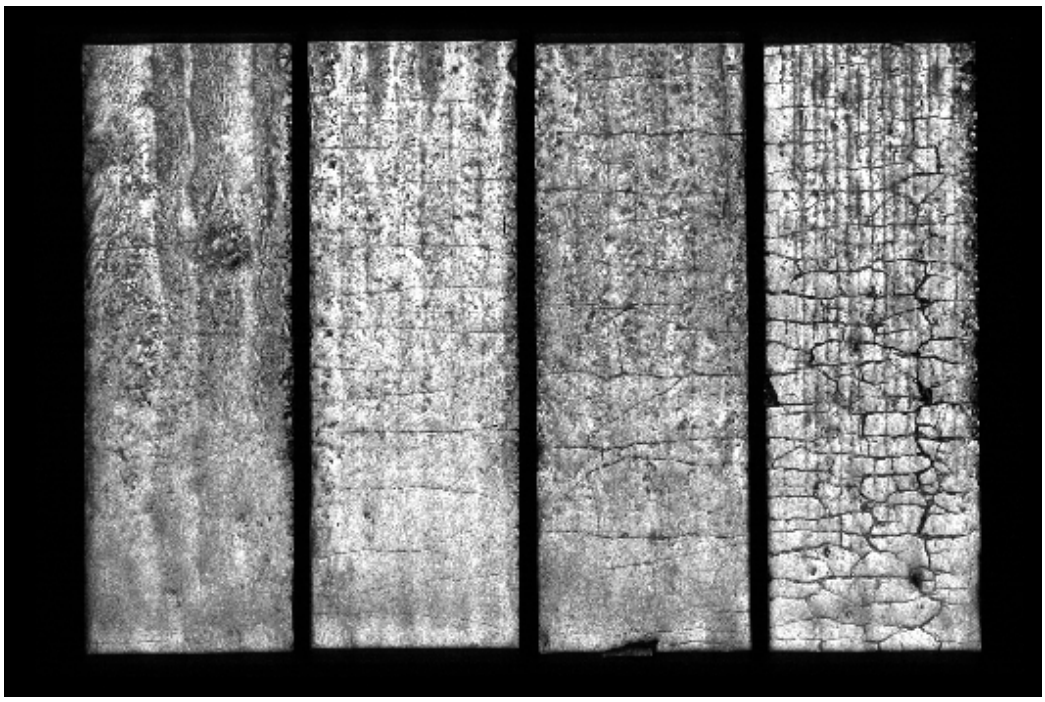

Figure 5.7(a): - The stationary jaw-crusher plates after crushing 1000kg of quartzite-bearing rock. The microstructures of the plates were, from left to right, hypoeutectic, eutectic to near-eutectic, hypereutectic (lvf) and hypereutectic (hvf).

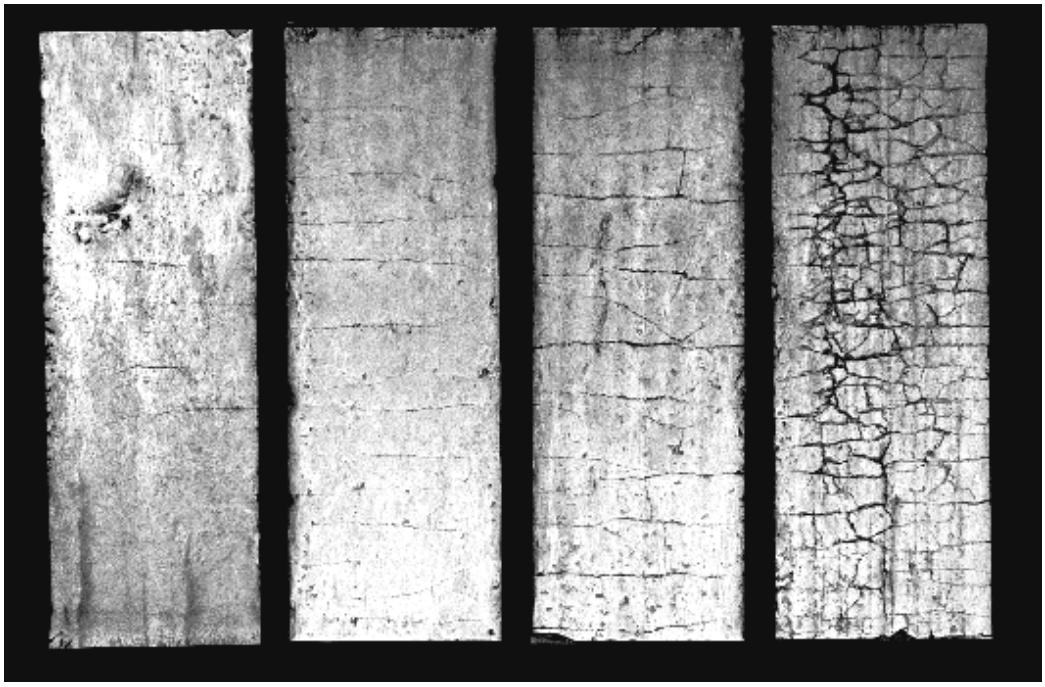

Figure 5.7(b): - The moving jaw-crusher plates after crushing 1000kg of quartzite-bearing rock. The microstructures of the plates were, from left to right, hypoeutectic, eutectic to near-eutectic, hypereutectic (lvf) and hypereutectic (hvf).

5.4 DISCUSSION

The heel plate and jaw-crusher experiments both demonstrated that the selection of welding parameters does affect the wear performance of an overlay. In each case, four overlay types were deposited on to the same substrate material with the same type of welding consumable. The geometry of each deposit was nearly identical but four different microstructures were produced. In both experiments there were differences in the wear performance of each deposit type, and they were observed in the form of spalling tendency.

The wear results revealed that the single-layer hypereutectic deposits exhibit a much greater spalling tendency than higher dilution deposits. The overlays with high volume fractions of primary carbides were most susceptible to this form of metal loss. This is possibly related to the reduction in fracture toughness that is likely to occur as the primary carbide volume fraction increases. Berns and Fischer (1986) studied hardfacing weld deposits and found that their fracture toughness data were adequately described by an energy model proposed by Chermant and Osterstock (1976). The model claims that the matrix is the most important factor in influencing the fracture toughness. Berns and Fischer treated the eutectic constituent as the matrix and found that, as the eutectic areas became smaller, so too did the fracture toughness. The eutectic areas and the resulting fracture toughness are likely to decrease significantly as the primary carbide volume fraction increases.

Hutchings (1992) described the role that material hardness and fracture toughness play in determining the apparent abrasion resistance of a material. He described how abrasive wear may occur by mechanisms dominated either by plastic deformation or

brittle fracture. If plastic deformation was dominant, the hardness of the counterface was said to be an important factor in determining its wear resistance. If, however, brittle fracture was dominant then the fracture toughness was said to be more important than the hardness. Based on the description given by Hutchings, one might expect that high-chromium white irons will generally provide excellent resistance to low-stress abrasion. In low-stress abrasion the hardness of the overlay is likely to be more important than its fracture toughness. However, as the applied stresses and the level of impact increase, so too will the importance of the fracture toughness of the overlay. Under conditions of high-stress abrasion the wear performance of a white iron deposit will also depend on such factors as the applied stresses, the hardness and size of the abrading materials, and whether these particles can penetrate and crack the carbides in the overlay. If the stresses are not too high, and if the carbides are harder than the abrading particles, then a low-dilution white-iron overlay may still perform very well. (This was seen in the results of pin-abrasion testing in chapter 4.) Under conditions of gouging abrasion, however, the levels of impact that are present are likely to ensure that the fracture toughness of the overlay is more important than its hardness. Consequently, low-dilution deposits are likely to wear at faster rates than deposits with higher dilutions, and this was seen in the heel plates and jaw-crusher experiments.

The fact that optimum wear performance was not provided by minimising dilution suggests that high-chromium white iron welding consumables were not the best selection for these applications. Articles by Menon (1996) and Zollinger *et al.* (1998) suggest that white-iron overlays are ideally suited to combat low-stress abrasion but are generally not recommended for use in conditions involving either high stresses or impact.

While the level of impact in these experiments may have been sufficient to expose the low fracture toughness of white-iron weld deposits, there are other possible explanations for the results. For example, the residual stresses in single-layer hypereutectic deposits are likely to be higher than the residual stresses in hypoeutectic overlays. One would expect that as the dilution decreases (and the differences in composition between the substrate and overlay increase) the residual stresses will increase. Thus the results may not be a characteristic solely of the wear performance of a hypereutectic microstructure, but rather a characteristic of the residual stresses that arise when there is an abrupt change in composition between two very dissimilar materials. If a hypereutectic layer had been deposited on to a high-dilution buffering layer, the reduction in residual stresses may have brought about a very different result.

Another issue arises in that the presence of the complex regular microstructure (shown in Figures 5.4) may have contributed to the poor wear performance of the strongly hypereutectic deposits. Very little is known about the mechanical properties of this structure.

The most important event in carrying out these experiments was the realisation that optimum conditions for the deposition of single beads may not correspond to the optimum conditions for multi-pass overlays. If the objective is to minimise dilution then, for single beads, this is equivalent to minimising the ratio of substrate melted to material deposited. For multi-pass overlays, however, the objective is to minimise the average penetration subject to the constraint that the average height of the overlay is fixed or specified. There is, therefore, a great need to build on the understanding of single-bead deposits by investigating the factors affecting the dilution of overlapping beads.